SPECTROSCOPY

A.Pospieszczyk

Forschungszentrum Jülich, Institut für Plasmaphysik, Assoziation EURATOM - FZJ
D-52425 Jülich, Germany
Tel. (49) 2461 61 5536, Fax (49) 2461 61 3331

ABSTRACT

A brief introduction into the spectroscopy of fusion plasmas is presented. Basic principles of the emission of ionic, atomic and molecular radiation will be explained and a survey of the effects, which lead to the population of the respective excited levels, will be given. The instrumentation, which is necessary for such measurements under the conditions in tokamak and stellarator plasmas, will be described. As illustrative examples for the wide wavelength range covered the derivation of core plasma parameters, transport properties, boundary temperatures and fluxes including their molecular composition will be given.

I. INTRODUCTION

Passive plasma spectroscopy can be a very powerful tool for the diagnostics of high temperatures plasmas. Without any interferences of probes or beams with the emitting species, information about the plasma state is transferred always nearly directly from the position of its origin. For example near the wall atomic as well as molecular spectroscopy tells us the amount and kind of particles, which enter the region of the confined plasma, whereas the central content can be derived from ionic lines of multiply ionized impurities. For nearly one century astrophysicists have already used the radiation from the sun and stars to obtain information about the status of these objects. There exists an excellent book, which compiles a lot of details in this respect[1] and describes many of the techniques, which nowadays are used for the interpretation of the measured spectra in laboratory plasmas.

The huge energetic range of emission from the X-ray to the infrared spectral range covers about 5 orders of magnitude (from fractions to several 1000 nm in the vacuum and the air) and requires, therefore, a variety of spectral apparatuses. However, the basic principles are nearly equal in their designs, although a lot of sophisticated technique is needed to achieve the desired goals.

II. ATOMIC AND MOLECULAR SPECTROSCOPY

II.1 Energy levels

Here we will give a brief description of the energy-level structure of atomic and molecular systems. There are many excellent textbooks treating this topic in the case of atoms[2,3,4,5,6,7] and molecules[8] and, therefore, we will deal more with qualitative aspects. The starting point for the calculation of the energy of an electron is the solution of Schrödinger's equation with an electron in a central field of a nucleus with a charge Z. The eigenvalues E_n come then out as a function of only the principle quantum number n:

$$E_n = R_y Z^2 / n^2 \qquad (1)$$

with R_y the Rydberg constant. In a more-electron system the field for the outer electron is no longer Coulombic but still central and the n has to be replaced by $n_{eff}=n-d$, where n_{eff} is called the effective quantum number , and d the quantum defect.

In the case of molecules other energies contribute to (1). This can be seen in fig.1:

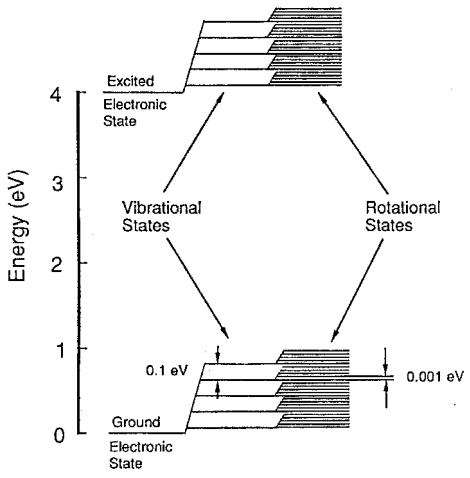

Figure 1: Schematic molecular energy level diagram

Apart from energy levels corresponding to different electronic arrangements, there are, for diatomic molecules, also different states corresponding to vibrational and rotational motions. In the case of polyatomic molecules, stretching and bending modes can additionally occur, which is not only a disadvantage, but can help for identification.

The additional vibrational and rotational energy is, in the case of an harmonic oscillator with a frequency ν_c and rigid rotation, expressed by:

$$E_{v,rot} = (v + 1/2)\, h\nu_c + BJ(J+1) \qquad (2)$$

where B is the (effective) rotational constant, and v and J the respective vibrational and rotational quantum numbers.

II.2 Radiative Transitions

Between an upper level E_i and a lower level E_j are three types of radiative transitions possible: spontaneous as well as stimulated emission and absorption, all with a frequency ν_{ij} given by:

$$h\nu_{ij} = E_i - E_j \qquad (3)$$

Spontaneous emission is characterised by a transition probability by unit time, A_{ij}. The other two depend on the presence of a radiation field and are more important in the interaction of a laser field with particles. In the case of dipole transitions, which have the largest values and are, therefore, called „allowed“, the life time of the state E_i, its transition probability into all lower states j and the often used so-called (absorption) oscillator strength are related by the following expression:

$$\frac{1}{\tau_i} = \sum_j A_{ij} = 8.0325\times 10^9 \frac{m}{\mu R_y^2} \sum_j \frac{g_i}{g_j} f_{ji} \qquad (4)$$

where the g_i and g_j are the statistical weights of the initial and final states participating in the transition. For an atom (3) gives normally rise to a single line or a well separated „bunch“ of lines (multiplets). However, in the case of molecules equation (2) leads to an appearance of many lines, the so-called „bands“. Transitions between the rotational levels lead to equidistant lines emitted in the far infrared (~100 μm), whereas those between vibrational levels result in lines in the near IR (~1 μm). The spectrum can be written:

$$\Delta E = h\nu_c + 2B\,(J+1)\ [-2BJ] \qquad (5)$$

with a so-called „R-branch“ and *[ ]* with a „P-branch“ for all J = 0, [1, 2, ...]. In transitions between different electronic configurations much higher energies are involved (~eV, visible and UV region) and lead also to bands, the intensities and the observed vibrational structure of which are explained by the „Franck-Condon principle[8]“. While ΔJ=0 is forbidden in a pure ro-vibrational transition, this can happen in the latter case and gives rise to an additional „Q-branch“.

III. COLLISION PHYSICS

III.1 Boltzman and Saha Equation

Under the conditions of (local) thermodynamic equilibrium (LTE), which means that all population and depopulation processes are in equilibrium with their reverse processes, the Boltzman equation gives the relative populations of two states of an atom (ion):

$$n_i / n_j = g_i / g_j \ \ exp(-\Delta E_{ij} / kT) \qquad (6)$$

where ΔE_{ij} is the energy difference between the two states. However, this is only applicable for electron densities

$$n_e \geq 7 \times 10^{18}\, (Z^7 / n^{17/2})\, (kT / Z^2 \chi_H)^{1/2}\ \mathrm{cm}^{-3} \qquad (7)$$

with χ_H the ionization energy of hydrogen[9]. For the excited levels with prinipal quantum numbers higher than this one, the Saha equation, which describes the intensity ratios of the spectra of different ionization levels n_z and n_{z+1} can be used:

$$\frac{n_{z+1,1} n_e}{n_{zn}} = \frac{g_{z+1,1}}{g_{zn}}\, x2\, \frac{(2\pi n_e kT)^{3/2}}{h^3} \exp\left(-\frac{\chi_{zn}}{kT}\right) \qquad (8)$$

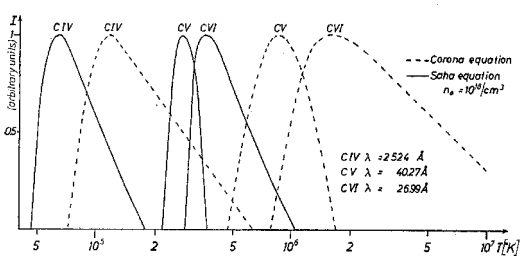

Figure 2: Relative carbon line intensities for different ionization stages as a function of temperature

III.2 The corona model

For the conditions of a fusion plasma with much lower n_e excitation by collisions is in equilibrium with de-population by radiation and the so-called corona model applies. In[10] a special solution for this problem is given, which introduces the so-called corona equation:

$$\frac{n_{z+1}}{n_z} \approx 10^8 \frac{\zeta}{n_0} \frac{1}{\chi_z^2} \frac{kT}{\chi_z} \exp\left(-\frac{\chi_z}{kT}\right) \quad (9)$$

with ζ the number of electrons in the outer shell. Fig. 2 illustrates the difference between equation (8) and (9) for carbon showing that the temperature required for the appearance of a line is considerably higher than in thermal equilibrium. Other effects can lead to additional shifts (see below).

Because the temperature in a fusion device usually increases from the edge to the centre we find increasingly higher ionization stages in more or less concentric narrow regions. Therefore, deviations from (9) may lead to a wrong radial positioning of the respective impurity.

IV. INSTRUMENTATION AND BASIC PROPERTIES

Spectral resolution instruments of different kinds are used for resolving the different wavelength components of the light. Important figures of merit for such devices are resolving power, light transmission and - presently more and more important - imaging quality. The most used type are grating spectrometers, as they often offer nearly all of these three properties simultaneously. Prism instruments, the Fabry-Pérot interferometer, and the Fourier transform spectrometer are mostly employed for special purposes.

IV.1 Grating spectrometers

The dispersion in these instruments is governed by the grating equation:

$$m\lambda = d\,(\sin\alpha + \sin\beta) \quad (10)$$

Here d is the line separation and α and β the angles of incidence and reflection, respectively. The resolving power $\mathcal{R}$ of the grating is determined by the total number of illuminated lines N and by the diffraction order m:

$$\mathcal{R} = \lambda / \Delta\lambda = N\,m \quad (11)$$

Normally a grating is ruled in a surface layer of aluminium on a substrate by means of a diamond tip. Replica gratings which are the ones that are marketed, are manufactured by a casting procedure. During recent years holographic gratings have been much used. These gratings are produced by recording interference fringes from two crossed laser beams. A density of up to 6000 lines/mm can be attained so that a 10 cm grating can have a resolving power of 6×10^5 in the first order. Also the line separation can be varied along the grating basis so that comfortable flat detectors can be used (see below).

The intensity that is diffracted at a certain wavelength depends on the shape of the lines. Ruled gratings are normally made with a certain *blaze* angle chosen according to which wavelength region is to be enhanced reflective action. The efficiency of such a grating can be up to 70% at the blaze angle for a certain order. An especially high resolution, but many overlapping orders at higher m, is obtained with an echelle grating. Such gratings operate at such a high angle that the steep side of the line is utilized and have comparatively few lines/mm but operate at a very high diffraction order so that resolving powers in the order of 10^6 can be obtained. More useful information can be found in[11].

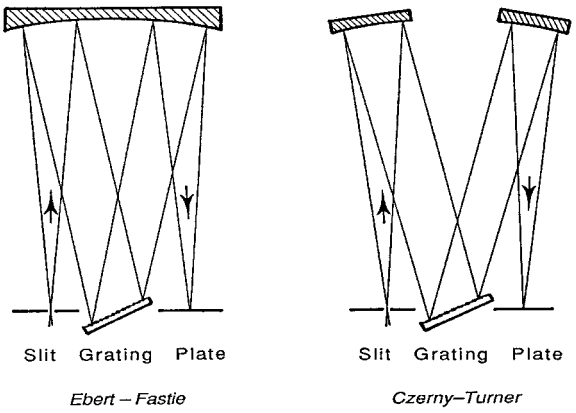

Figure 3: two common arangements for the visible spectral range

Spectrometers are, in general, equipped with mirrors instead of lenses. Some common, compact, arrangements are shown in figure 3. Because of their symmetrical set-up both types are almost free from coma. However, the Ebert-Fastie mounting with its spherical mirror has no imaging qualities, whereas the Czerny-Turner type is in this direction more flexible as the 2 individual mirrors can have different (toroidal) shapes.

By using concave gratings the need for collimating and focussing mirrors is eliminated, which is particularly valuable in the VUV (vacuum ultraviolet) and XUV (extreme UV) regions where conventional mirrors are ineffective. For the very short wavelengths that are obtained in spectra from highly ionized atoms or in X-ray spectra, a grazing angle of incidence (fig.4) is used to minimize the absorption losses in the grating.

By choosing a special toroidally curved grating and a ruling technique with varying line spacings the recording plane can be made nearly flat so that large, plane detectors can be used. Such types, which can cover ranges from about some 10 Å to 2000 Å are referred to as SPRED-spectrometers[12] (survey, poor resolution, extended domain) and are very valuable instruments for monitoring the central plasma impurities (see next paragraph).

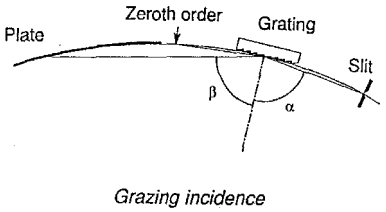

Figure 4: arrangement for small λ

IV.2 Detectors and calibration

Photographic plates are two-dimensional detectors; therefore, they are still very valuable for survey work and have a high information density. However, for time dependent measurements, photoelectric detectors have to be used. A very low noise level unit is the *photomultiplier tube (PMT)*, which consists of a cathode sensitive from the IR down to VUV and a chain of dynodes for electron multiplication purposes. However, a PMT is a zero-dimensional unit, which can only monitor one wavelength simultaneously. Recently also multi-cathode arrangements have been develloped, which can overcome this problem[13]. Another solution are the *charge coupled devices (CCD's)*, which consist of an array or matrix of photosensitive elements (pixels). They can have quite a high quantum efficiency and combine high sensitivity with high spatial resolution. In the linear case the pixels can be even rectangular with sizes of some 10μ time a couple of mm. In order to obtain an even higher light sensitivity the arrays or chips can be placed behind an *image intensifier tube*[14], which is based on a *microchannel plate*. The electrons from a cathode are multiplied along the channel, propelled by an applied electric field. The electron showers that are spatially arranged corresponding to the primary image impinge on a phosphor screen which produces an amplified image of the original spectrum. The light is then transferred to the detector with retained spatial information, employing optical fibers or optics. An amplification of more than 10^4 can be obtained. A method, which combines both the advantages of a CCD and a noise free amplification is the latest technology of CCD electron multiplication (EMCCD). The unique feature is an electron multiplying structure (gain register (see fig.5)). It is similar to the shift register except that one of the electrodes is replaced by two electrodes. The high electric field applied causes impact ionization and leads to electron multiplication. When executed over a large number of transfers, a substantial gain of about 10^3 is achieved with no loss mechanism. Because of the huge number of information, which can easily reach the Gbyte range, some restrictions as time resolution and/or storage space may apply for the latter systems.

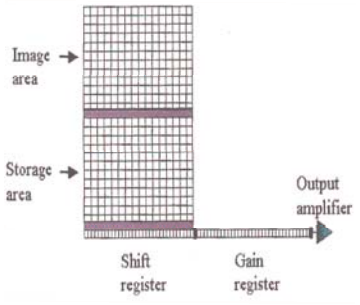

Figure 5: Simplified structure of Andor's[15] EMCCD sensor

There are several lamps which can be used for absolute intensity calibrations of the systems used. However, most of them are only applicable for wavelengths above 100nm and are mostly based on thermal sources with very high temperatures. *Tungsten ribbon lamps* are mostly operated at temperatures around 3000K with a maximum of the emission at 1μm and can be used above 400nm. Higher temperatures (about 4000K) are reliably supplied in the anode crater of a *carbon arc*. An alternative for UV and XUV applications is provided by the NBS *argon mini arc* source[16], which emits light down to 130nm In ranges below 100nm intensities for selected wavelengths can be calibrated by the *branching ratio method*[17], which uses pairs of spectral lines of an atom or ion the upper level of which is identical. One of the lines should be in the visible spectral range, the other one at shorter wavelengths where the calibration is desired.

IV.3 Line widths

The natural line widths for lines emitted in fusion plasmas can practically always be neglected. Much more important is the thermal movement of the particles, which leads to a *Doppler shift* of an emitted line (see V). Averaged over an Maxwellian ion velocity distribution the resulting Gaussian line shape has a half width (FWHM) of:

$$\Delta\lambda = \frac{(2k\ln 2)^{1/2}}{c}\sqrt{\frac{T}{M}}\lambda_0 = 7.16\cdot 10^{-7}\sqrt{\frac{T}{M}}\lambda_0 \qquad (12)$$

which can serve for ion temperature determinations. In practice other line broadening mechanisms can cause immense problems or the distribution functions are asymmetric, especially from atoms near wall. However, their measurement might also help to identify the interaction processes. For instance, particles released by desorption, chemical sputtering or even evaporation give considerably smaller line profiles than those reflected or physically sputtered from the limiter.

The *Zeman effect*, which is effective in the presence of a magnetic field *B* leads to line splittings of:

$$\Delta\lambda = \frac{eB}{4\pi\, m_e c}\lambda^2 (M_1 g_1 - M_2 g_2) \qquad (13)$$

with g_J as the Landé factor in LS-coupling:

$$g = 1 + \frac{J(J+1)+S(S+1)-L(L+1)}{2J(J+1)} \qquad (14)$$

giving rise to the appearance of π- resp. σ-components with different polarization. In order to minimize the influence of the splitting it is in practice advisable to choose lines with Δm=0 or equal quantum numbers L,S and J so that the splitting for the π-component is to a first approximation zero. Small shifts caused in the second approximation by the Paschen-Back effect[2] have sometimes to be taken into account.
External electric fields E can also give rise to level splittings due to the *Stark effect* according to:

$$\Delta\lambda_{JM} = E^2 (A_{LJ} + B_{LJ} M^2) \qquad (15)$$

A and B depending on L and J[6], which can result in complicated line broadenings depending on the excitation mechanisms. In practice noticeable splittings only take place in the case of electric fields larger than 1 keV/cm, which are rarely reached - mostly only during external biasing, are convoluted with Zeman and Doppler broadening and require very high spectral resolution. Therefore, it is advisable to measure those fields indirectly e.g. by line shifts caused by directed motions (see V).

V. PLASMA DIAGNOSTICS

Plasma spectroscopy allows the determination of a number of parameters such as ion and electron temperatures, distribution of charge states from which the impurity transport can be deduced, plasma rotation which tells us something about internal fields, particle fluxes, their penetration depths and velocity distributions which determine the fuelling and the impurity content. It is nearly impossible to deal with all of these in detail. Therefore, only some representative examples can be given.

V.1 Core measurements

Measuring the intensities and regions of origin of spectral lines provides information on the location of the element under study. For the reconstruction of the location of the emission from line integrating , passive measurements presently two methods are in use. Tomography, which requires a number of lines of sight over the plasma radius, and a complicated mathematical algorithm[18], and modelling describing the impurity ion distribution taking into account their transport and the temperature profile.

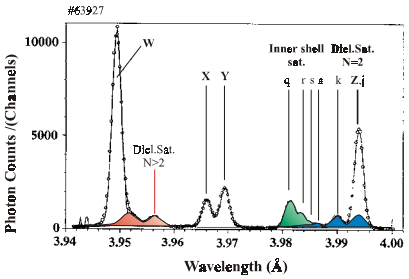

Key	Transition	Wavelength (Å)*
W	$1s^{2\,1}S_0 - 1s2p\,^1P_1$	3.9494
X	$1s^{2\,1}S_0 - 1s2p\,^3P_2$	3.9661
Y	$1s^{2\,1}S_0 - 1s2p\,^3P_1$	3.9696
q	$1s^2 2s\,^2S_{1/2} - 1s2s2p\,(^1P)\,^2P_{3/2}$	3.9815
r	$1s^2 2s\,^2S_{1/2} - 1s2s2p\,(^1P)\,^2P_{1/2}$	3.9836
a	$1s^2 2p\,^2P_{3/2} - 1s2p^{2\,2}P_{3/2}$	3.9860
k	$1s^2 2p\,^2P_{1/2} - 1s2p^{2\,2}D_{3/2}$	3.9901
j	$1s^2 2p\,^2P_{3/2} - 1s2p^{2\,2}D_{5/2}$	3.9941
Z	$1s^{2\,1}S_0 - 1s2s\,^3S_1$	3.9944

* Theory by Vainshtein and Safranova

Figure 6: Spectrum of ArXVI-XVIII in the X-ray region

Figure 6 displays a spectrum, which contains lines from 3 ionization state of argon. This gas, the helium-like state of which (ArVXII) is the dominant charge state in the range from 0.5to 3.5 keV, has been puffed into a plasma discharge for diagnostic purposes[19]. Several plasma parameters have been deduced from these spectra.
The *intensity ratio* between the resonance line w and the dielectronic satellite k line provides the *electron temperature* because of the different temperature dependence of the origin of these two lines (dielectronic recombination is a recombination process, which involves 2 electrons simultaneously)[20]. Other line ratios, which all use equation (9), can be obtained from similar spectra in the visible to the XUV depending on the degree of ionization. Extensive wavelength tables have been compiled for reference[21,22]. Also the Internet provides wavelengths[23,24,25] and transition probabilities are also available[26,27].
The *line shifts* can be used for *plasma movements* exploiting the Doppler effect:

$$\Delta\lambda / \lambda = \upsilon / c \qquad (16)$$

with c=3x10^8 m/sec. As these movements are generally in the order of 10^3 to 10^4 m/sec, instruments with a resolution of about at least 10^5 are required for accurate measurements! A special movement is the *plasma rotation*, which can serve for the determination of the internal radial electric field E_r, as this, the density gradient and the poloidal and toroidal fields are connected via :

$$E_r = - \partial p_i / eZ_i n_i \partial r + (B_{pol} v_{tor} - B_{tor} v_{pol}) \qquad (17)$$

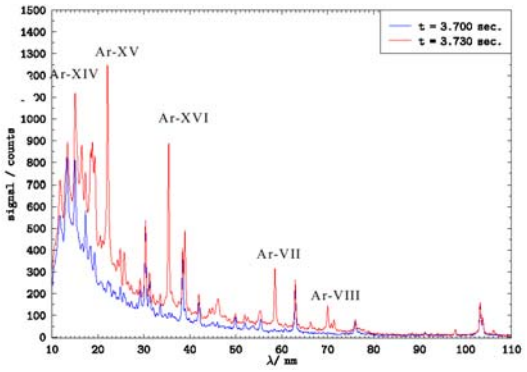

Figure 7: Argon lines in the XUV during a puff recorded by a SPRED- spectrometer.

In[12] the spectra shown in fig.6 have been used for such measurements as well as for the determination of *ion temperatures* via *line width* measurements (see also below).

Also *transport properties* can been deduced from similar gas puffs experiments. The time evolution of spectroscopic signals from different ionization stages of argon (Ar-I,-VIII,-X,-XII,-XIV,-XV,-XVI,-XVII) - a spectrum from a SPRED-spectrometer is shown in fig.7 - was recorded with high time resolution (0.3...1 ms)[28] (fig.8).

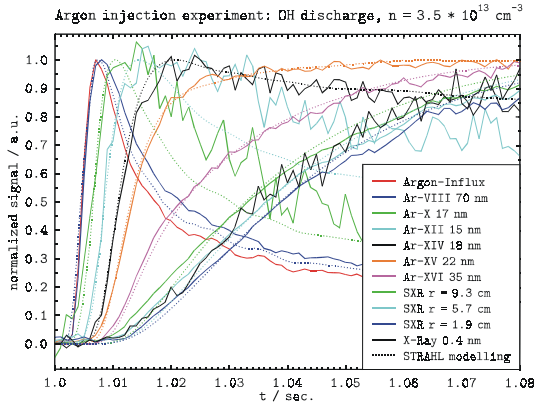

Figure 8: Measured line intensities and STRAHL results (dotted lines). The higher ionisation states extend consecutively from left to right and down in the line captions.

This kind of spectrometer is very useful for such investigations, as it is important to obtain as many information as possible during one discharge. The *modelling* of the rise and decay times by a descriptive code (STRAHL) then yields the diffusion and the (inward) drift velocity of the argon. These numbers are important to judge the impurity concentration for different plasma parameters.

V.2 Boundary measurements

For the purpose of the diagnostics of edge plasmas, optical methods are one of the favored tools as they offer the possibility of obtaining information without no or relatively less interference of the technique itself and the observed quantities. The range to be covered is determined by the ionization length of atomic hydrogen and is characterized by $10^{11}\mathrm{cm}^{-3} < n_e < 10^{13}\mathrm{cm}^{-3}$, $1\ \mathrm{eV} < T_e < 100\ \mathrm{eV}$, $10^{-3}\, n_e < n_I < 10^{-1}\, n_e$, $n_{Ho} \approx 10^{-3}\, n_e$. As the gradients in this part of the plasma are relatively steep (of the order of 1cm) and may also vary with toroidal and poloidal location, observations have to be performed within a spatial resolution of about one millimeter and at numerous positions around the discharge vessel.

The emission coefficient for a spectral line from an excited level of a species A with density n_A^* is given by:

$$\varepsilon = \frac{1}{4\pi} n_A^* A_{ij} \qquad (18)$$

However, this is normally not what one wants to know; more important is the number of particles in the ground state. If one assumes again coronal conditions (equilibrium between excitation (by electrons) into the excited levels from the ground state n_A and deexcitation by radiation into all lower states) i.e.:

$$n_A \sum_{k \le i} A_{ik} = n_A\, n_e < \sigma_{Exg}\, \upsilon_e > \qquad (19)$$

where $\Sigma_{k \le i}\, A_{ik}$ is the transition probability from level i into all lower states k and $<\sigma_{Exg}\upsilon_e>$ the excitation rate coefficient by electron collisions from the ground state (a function of T_e), we obtain in terms of the branching ratio $\Gamma = A_{ik} / \sum_{k \le i} A_{ik}$:

$$\varepsilon = \frac{\Gamma}{4\pi} n_A\, n_e < \sigma_{Exg} \upsilon_e > \qquad (20)$$

or for the line integrated intensity

$$I_{tot} = \Gamma \frac{h\nu}{4\pi} \int_{r_1}^{r_2} n_A(r) n_e(r) < \sigma_{Exg}\, \upsilon_e > dr \qquad (21)$$

where $n_A(r)$ is the impurity density profile and $n_e(r)$ the electron density profile.

The flux $\Phi(r)$ of atoms with a velocity υ_A into a plasma, which is assumed to be equivalent to the numbers of ionization events, is governed by the relation:

$$\frac{d\Phi_A}{dr} = \frac{d(n_A \upsilon_A)}{dr} = -n_A(r) n_e(r) < \sigma_I \upsilon_e > \qquad (22)$$

or (integrated over the whole attenuation length):

$$\Phi_A = \int_{r_1}^{r_2} n_A(r) n_e(r) < \sigma_I \upsilon_e > dr \qquad (23)$$

By taking the ratio of equation (21) and (23), one obtains a relation for the flux ϕ_A as function of the measured total intensity:

$$\Phi_A = 4\pi \frac{I_{tot}}{\Gamma h\nu} \frac{\int_{r_1}^{r_2} n_A(r) n_e(r) < \sigma_I \upsilon_e >_{(r)} dr}{\int_{r_1}^{r_2} n_A(r) n_e(r) < \sigma_{Exg} \upsilon_e >_{(r)} dr} \qquad (24)$$

In this way the integrated photon emission along the penetration path into the plasma is a measure for the amount of flux of released particles per unit length of the source, provided that the atoms (or molecules) are completely ionized further (or dissociated) by electron collisions within the line of sight[29]. The total number of particles is then obtained by multiplication with the whole length of emitting components. A more extensive derivation of formula (24) can be found e.g. in[30]. One should note here especially that a general solution of equation (7) is only possible, if $n_e(r)$, $<\sigma_I \upsilon_e>=f_i(r)=f(T_e)$, and $<\sigma_{Exg} \upsilon_e>=f_{ex}(r)=f_{ex}(T_e)$ are precisely known at the position of the corresponding measured intensities. Since the latter condition is mostly not fulfilled because of problems of access for the relevant diagnostics, an iterative procedure is required in general!

For this reason and provided the ratio $<\sigma_I \upsilon_e>/<\sigma_{Exg} \upsilon_e>$ has only a weak spatial (i.e.temperature) dependence in the region of interest, a simpler version of equation (24) can be derived:

$$\Phi_A = \frac{4\pi}{\Gamma} \frac{I_{tot}}{h\nu} \frac{<\sigma_I \upsilon_e>}{<\sigma_{Exg} \upsilon_e>} = 4\pi \frac{I_{tot}}{h\nu} \frac{S}{XB} \qquad (25)$$

where the following identities are valid: $S \equiv <\sigma_I \upsilon_e>$, $X \equiv <\sigma_{Exg} \upsilon_e>$, and $B \equiv \Gamma$. The expression on the right side of this equation is also often referred in this way in the literature in respect to flux determination from integral line intensity measurements[31].

The expression S/XB, which is needed to determine the absolute fluxes, is plotted in fig.9 as a function of T_e for different elements and lines[30]. In cases where the individual cross sections have not been obtained experimentally (which for neutrals is often the case), the excitation rates are calculated either by the formula of [32]:

$$< \sigma_{Exg} \upsilon_e >= 32 \cdot 10^{-8} f \left(\frac{R_y}{\Delta E}\right)^{\frac{3}{2}} \left(\frac{\Delta E}{T}\right)^{\frac{1}{2}} \exp\left(-\frac{\Delta E}{T}\right) \bar{g}\left(\frac{\Delta E}{T}\right) \qquad (26)$$

where f is the oscillator strength and $\bar{g}(\Delta E/T)$ the „effective Gaunt factor“ (T is expressed in eV). It is obvious that this formula can only be used, provided the upper level of the transition can decay by electric dipole radiation into the ground state (an optically allowed line).

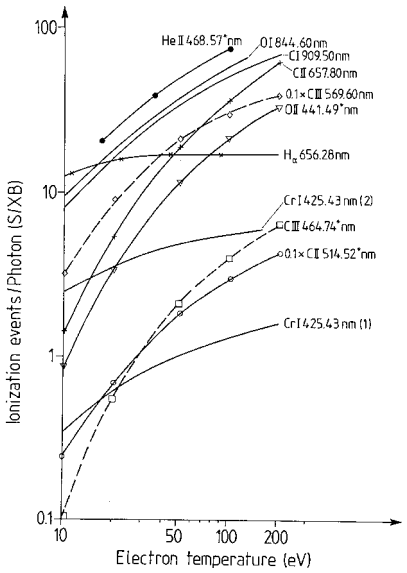

Figure 9: S/XB (ionization events per photon) for a number of atoms and ions

For CrI two curves are shown in fig.9 derived by two different models. Factors of 5 can easily be found between the different calculations, which often complicates the quantitative analysis.

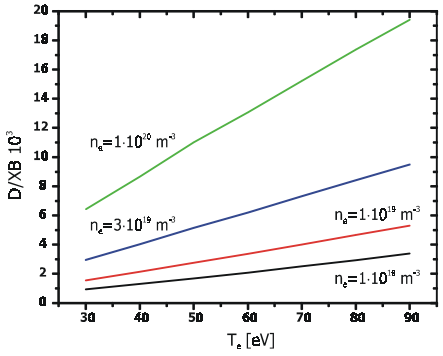

Figure 10: D/XB for the Fulcher-band emission of H_2

Another problem in the interpretation of the data arises when the particles enter the plasma predominantly in the form of molecules, but lines of the dissociated atomic species are (or have to be) observed. Several theoretical (e.g.[33,34]) and experimental (e.g.[35,36]) attempts have already been performed in the past in order to study the different contributions in the radiation of $H_\alpha(D_\alpha)$ from hydrogen atoms and molecules because of the importance of this element in fusion research. A number of 33 was deduced

(for a ratio H_i^0/H_α) about double as high as for pure atomic influx. This would mean that in the case of strong molecular hydrogen influx from wall and limiter (e.g. near the density limit or a "detached plasma"), the fuelling will be considerably underestimated. Recently the D/XB- value (the S/XB for molecules) for the Fulcher-band emission of molecular hydrogen has been calculated (fig.10) and experimentally confirmed, which now also allows the direct determination of the hydrogen-flux from tedious , high resolution molecular spectroscopy.

REFERENCES

1. A.Unsöld, *Physik der Sternatmosphären*, Springer; Berlin, 1955
2. E.U.Condon and G.H.Shortley, *The Theory of Atomic Spectra*, Cambridge University Press. New York, 1951
3. R.D.Cowan, *The Theory of Atomic Structure and Spectra,* UCP, Berkeley, 1981
4. H.G.Kuhn, *Atomic Spectra,* Academic Press, New York, 1962
5. B.W.Shore and D.H.Menzel, *Principles of Atomic Spectra,* Wiley, New York, 1968
6. I.Yu. Sobelman, *Atomic Spectra and Radiative Transitions,* Springer Verlag, Berlin, 1992
7. Shevelkov and L.A.Vainshtein, *Atomic Physics for Hot Plamas*, IoP, Bristol,1981
8. G.Herzberg, *Molecular Spectra and Molecular Structure.*
   a) *I The Spectra of Diatomic Molecules* , Van Nostrand, Princeton 1963
   b) *II Infrared and Raman Spectra of Polyatomic Molecules* , Van Nostrand, Princeton,1965
9. H.R.Griem, *Plasma Spectroscopy*, McGraw Hill, New York, 1964
10. G.Elwert, Zeitschrift für Naturforschung, 7a (1952) 432
11. M.C.Hutley, *Diffraction Gratings* (Academic, London, 1982)
    Handbook of Diffraction Gratings, Ruled and Holographic (Jobin-Yvon Optical Systems, 20 Highland Ave., Metuchen, NL, 1970)
12. R.J.Fonck, A.T.Ramsey, and R.V.Yelle, Applies Optics, 21 (1982) 2115
13. Hamamatsu Photonics, Hamamatsu City, Japan
14. Proxitronic GmbH, R.BoschStr., D-64625 Bensheim, Germany
15. Andor Technology, 9 Millenium Way, Belfast BT12 7AL Northern Ireland
16. J.M.Bridges and W.R.Ott, Applied Optics 16 (1977) 367
17. W.Whaling in: *Beam Foil Spectroscopy*, Vol. 2, I.A.Sellin and D.J.Pegg eds, Plenum Press, New York, 1976
18. L.C. Ingesson *et al*., Proc. EPS 1997, Part I, pp. 113 and references therein
19. G.Bertschinger, W.Biel, the TEXTOR-94 team et al., Physica Scripta, T83 (1999) 132
20. A.Gabriel, Mon.Not.R.Astron.Soc. 160 (1972) 99
    A.Pospieszczyk, Astron.&Astrophys. Vvv (1975) nnn
21. R.L.Kelly and L.J.Palumbo, *Atomic and Ionic Emission Lines below 2000 Å*
22. A.R.Striganov and N.S.Sventitskii, *Tables of Spectral Lines of Neutral and Ionozed Atoms*, Atomizdat, Moscow, 1966
23. National Institute of Standards and Technology, Physics Laboratory, http://physics.nist.gov/PhysRefData/Contents
24. R.L.Kelly, http://cfa-www.harvard.edu/amp/data/stats/kelly
25. Kurucz, http://leanda.pmp.uni-hannover.de/projekte/kurucz
26. W.L.Wiese et al., *Atomic Transition Probabilities*, Nat.Stand. Ref. Data Ser. Vol.I, Washington, 1966
27. V.G.Pa'lchikov and V.P.Shevelko, *Reference Data on Multicharged Ions*, Springer Verlag, Berlin, 1995
28. W. Biel, I. Ahmad, C. J. Barth, G.Bertschinger, Proc. EPS 2001, paper 4.015
29. M.F.Stamp, K.H.Behringer, M.J.Forrest, P.D.Morgan, H.P.Summers, Proc. 14th Europ. Conf. Contr. Fus. Plasma Phys., Budapest (Hungary), 1985, Vol.II, 539
30. P.Bogen, H.Hartwig, E.Hintz, K.Höthker, Y.T.Lie, A.Pospieszczyk, U.Samm and W.Bieger, J. Nucl. Mat., 128 & 129 (1984) 157
31. K.H.Behringer, J.Nucl.Mater., 145-147 (1987) 145
32. H. van Regemorter, Astrophys. J. 136 (1962) 906
33. D.H.McNeill, J. Nucl. Mater. 162-164 (1989) 476
34. K.Sawada, K.Eriguchi, T.Fujimoto, J.Appl.Phys. 73 (1993) 8122
35. D.A.Vroom and F.J.de Heer, J.Chem.Phys. 50 (1969) 580
    G.A.Khayrallah, Phys.Rev. A 13 (1976) 1989
    B.L.Carnahan and E.C.Zipf, Phys.Rev. A 16 (1977) 991
36. A. Pospieszczyk, Y.Ra, Y. Hirooka, R. W. Conn, R. Doerner, L. Schmitz, UCLA-PPG-1251, (Dec. 1989)